Electronic Supplementary Material (ESI) for Physical Chemistry Chemical Physics.

Supplemental Information for Isomer-Selected Ion-Molecule Reactions of Acetylene Cations with Propyne and Allene

P. C. Schmid,[1,2] J. Greenberg,[1] T. L. Nguyen,[3] J. H. Thorpe,[3] K. J. Catani,[1] O. A. Krohn,[1] M. I. Miller,[1] J. F. Stanton,[3] and H. J. Lewandowski[1,*]

[1] *JILA and the Department of Physics, University of Colorado, Boulder, Colorado, USA*

[2] *I. Physikalisches Institut, Universität zu Köln, Zülpicher Str. 77, 50937 Köln, Germany*

[3] *Quantum Theory Project, Departments of Chemistry and Physics, University of Florida, Gainesville, Florida, USA*

[*] Corresponding Author

S1. EXPERIMENTAL METHODS

A. Initial Coulomb crystal conditions

The starting point in any reaction measurement requires a pure bi-component Coulomb crystal of Ca^+ and $C_2D_2{}^+$, as shown in the inset of Figure 1 in the main text and in Figure S1 below with its corresponding mass spectrum. While recording a complete set of data for a single reaction curve, the initial number of Ca^+ and $C_2D_2{}^+$ ions are regularly confirmed to remain constant by analyzing the data from t = 0 bi-component Coulomb crystals using the TOF-MS. Mass spectra associated with t=0 correspond to samples of $C_2D_2{}^+$ that have not been exposed to C_3H_4. The ion numbers at t = 0 constitute the initial time point t = 0 in the reaction curves (Figures 2 and 3).

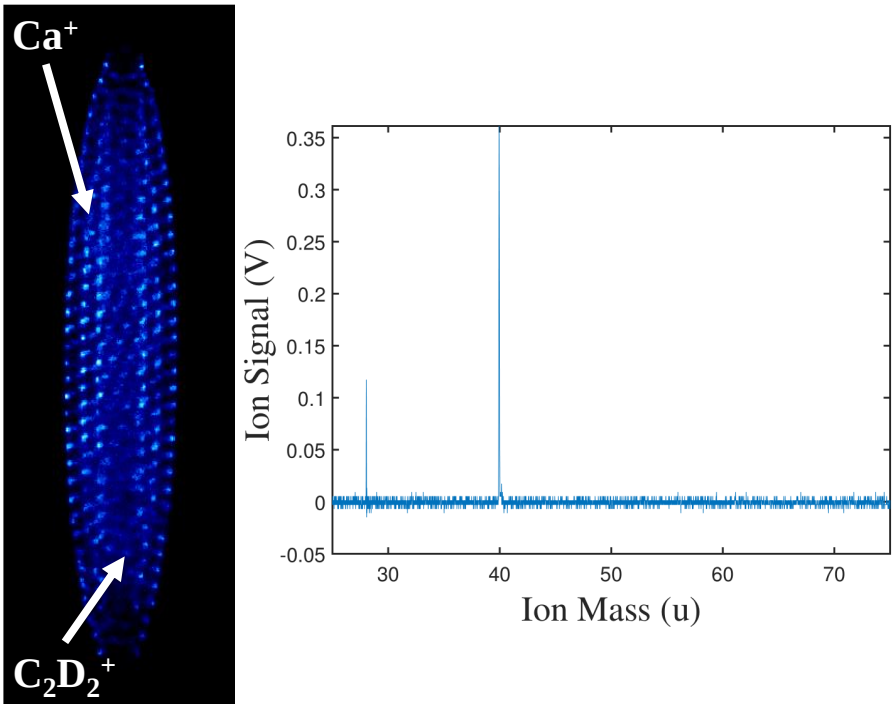

FIG. S1. Left: False-color fluorescence image of a typical t = 0 bi-component Coulomb crystal and its corresponding TOF-MS trace (right). The TOF-MS data were produced by a single load of the trap, i.e., not averaged over multiple experimental cycles. The number of reactant ions in the mass spectrum is determined by integrating the peak at mass 28 and corresponds to ∼140 $C_2D_2{}^+$ ions, co-trapped with ∼870 Ca^+ ions.

In the example mass spectrum in Figure S1, only $C_2D_2{}^+$ and Ca^+ are detected with

essentially no contaminant ions present. This clean starting condition allows for the identification of all detected products as coming from the studied reaction $C_2D_2^+$ with propyne or allene and not from contaminant ions. Thus, no unidentified, and therefore unaccounted for, reaction channels have to be taken into account in the analysis of the reaction kinetics.

B. Reaction spectrum

After the initial loading of the bi-component crystal, the neutral reactant gas (either DC_3D_3 or $H_2C_3H_2$) is introduced into the vacuum chamber for variable reaction times. Charged reaction products (of any order) accumulate in the trap during this time. Upon reaching the desired reaction time, the Coulomb crystal is ejected into the TOF-MS and the corresponding mass spectrum is recorded. Figure S2 displays an example spectrum from the reaction $C_2D_2^+ + DC_3D_3$ after 180 seconds. Products of this reaction are readily identified as new peaks that were not present in the initial t = 0 spectrum (compare to Fig. S1). Chemical formulae are assigned to the product peaks based on their measured mass. The number of ions in each product channel is calculated by the integration of each product channel peak, as discussed in a previous publication [1]. By repeating this step for all possible reaction times, the corresponding reaction curves (Figures 2 and 3) can be created.

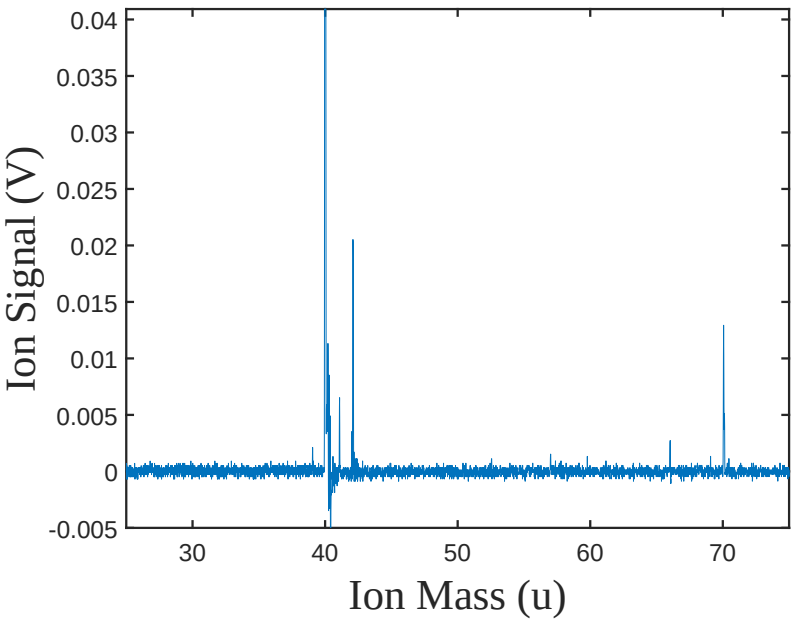

FIG. S2. Example mass spectrum from the reaction $C_2D_2^+ + DC_3D_3$ after 180 seconds. While no residual $C_2D_2^+$ ions are observed (mass 28), the formation of the major product masses 42 u and 70 u can be identified. Their assigned chemical formulae are $C_3D_3^+$ and $C_5D_5^+$. The number of product ions, determined by peak integration, are roughly 47 and 23 ions, respectively. Note that the intensity of Ca^+ (mass 40) is cut-off in this spectrum due to its large ion number (>800 ions). Due to the high detection sensitivity of our apparatus, we are sensitive to random ions from reactions with the background. Here the peaks at 41 u and 66 u are present in this single mass spectrum only, thus can be neglected in the determination of the reaction kinetics of $C_2D_2^+ + DC_3D_3$.

C. Higher order products

Charged reaction products are accumulated in the ion trap as the reaction progresses and can react further with excess neutral reactant present in the chamber. The measured reaction curves exhibit unique characteristics that enable the assignment of a given product order. An example of multiple product order – primary, secondary, and tertiary – detection from the reaction $C_2D_2^+ + DC_3D_3$ is shown in Figure S3. $C_5D_5^+$ represents the primary reaction channel, while $C_6D_5^+$ is the result of the reaction $C_3D_4^+ + DC_3D_3$. The tertiary-order product $C_7D_7^+$ is likely the result of the reaction $C_6D_5^+ + DC_3D_3$, as evident from

the delayed onset in growth. While the downturn in $C_6D_5^+$ ion numbers at late reaction times would support the suggested pathway (see Figure S3), there are further second-order products with similar reaction behavior that could contribute to $C_7D_7^+$. Additional observed tertiary products could result from $C_6D_5^+ + DC_3D_3$. However, we cannot uniquely confirm the specific reaction pathways, as the details of these higher order reactions are beyond the scope of this investigation.

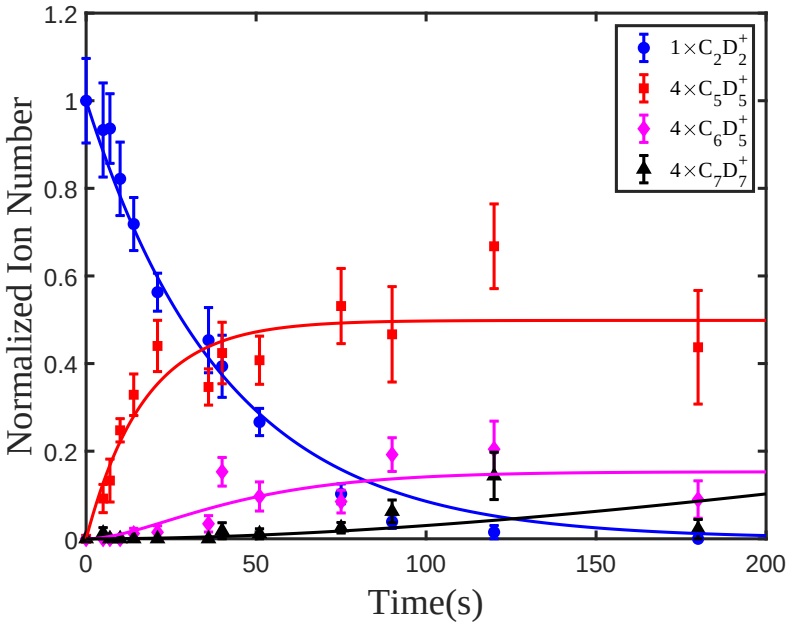

FIG. S3. Reaction curves for three products observed in the the reaction $C_2D_2^+ + DC_3D_3$. Product ion numbers are normalized to the initial number of $C_2D_2^+$ in the reaction, ~150, and multiplied by four so they can be seen on the same scale as acetylene. The corresponding reaction order for each of the three products is evident by the delayed onset of ion accumulation. Solid lines represent fits to primary, secondary, and tertiary reaction product models.

D. Total ion measurements

As in previous measurements, the total ion number in the ion trap is measured throughout the reaction. This is an important measurement in order to make sure no ions are lost from the trap, which would result in systematic errors in the kinetic analysis. Every time a Coulomb crystal is ejected into the TOF-MS, the number of ions in all mass peaks up to mass 140 u is summed up with the exception of mass 40 (Ca^+). Mass 40 is not included in

this analysis, since the high abundance of Ca^+ makes it difficult to detect small changes in ion numbers. By plotting the total ion number as a function of reaction time, ion losses can be readily detected. Figure S4 presents the total ion data for the $C_2D_2{}^+ + DC_3D_3$ reaction shown in Fig. 2 in the main text. Similarly, Fig. S5 shows the total ion data for the $C_2D_2{}^+ + H_2C_3H_2$ reaction shown in Fig. 3 in the main text. In both cases, no ion losses are detected for the measured reaction times. This shows that no unaccounted for reaction channels are present in the data, thus supporting the proposed reaction mechanism (see Figures 4, 5 in the main text).

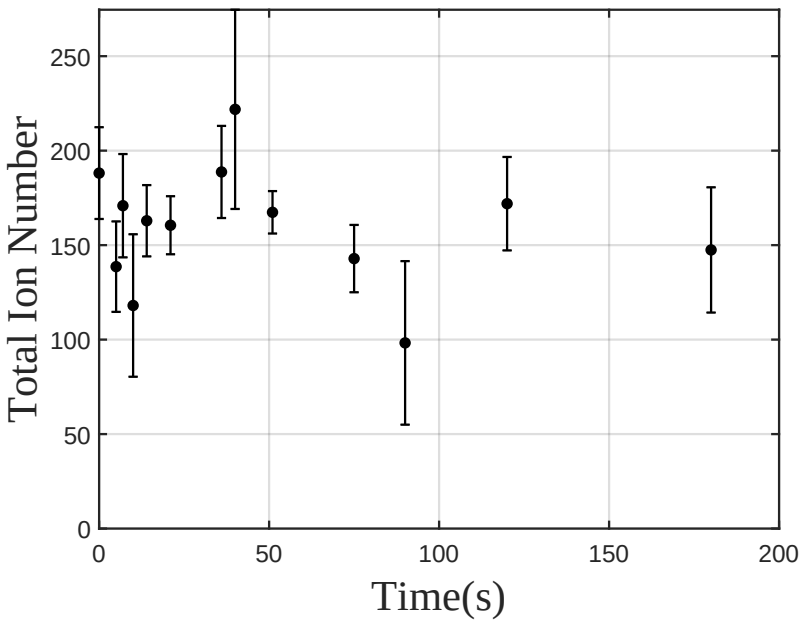

FIG. S4. Total summed ions from all detected product and reactant channels as a function of reaction time for the $C_2D_2{}^+ + DC_3D_3$ reaction presented in the main text. These numbers include reactants and products of all orders (primary, secondary, tertiary) observed in the experiment, but exclude Ca^+. The slope of a fit through the data (not shown) is statistically consistent with zero (-0.1 $\pm$ 0.3 at 90% confidence interval), indicating no ion loss.

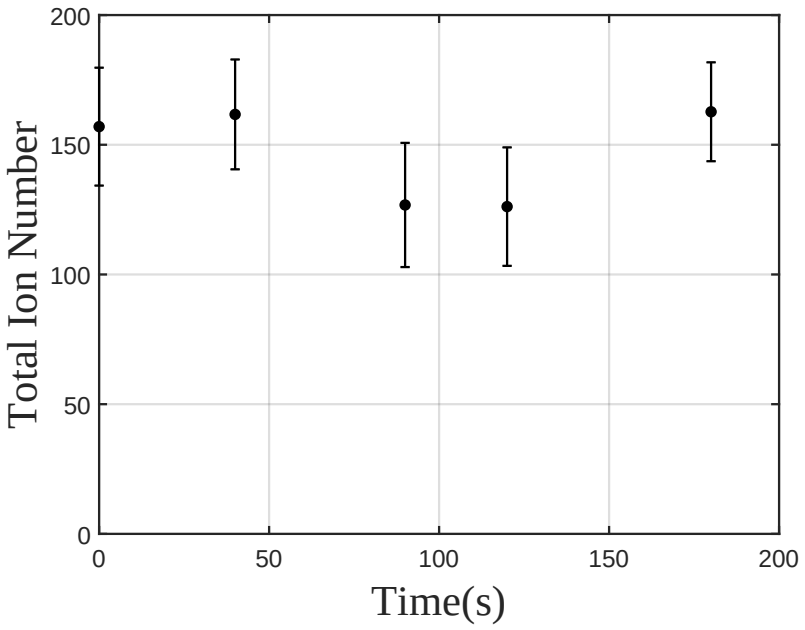

FIG. S5. Total summed ions from all detected product and reactant channels as a function of reaction time for the $C_2D_2{}^+ + H_2C_3H_2$ reaction presented in the main text. These numbers include reactants and products of all orders (primary, secondary, tertiary) observed in the experiment.The slope of a fit through the data (not shown) is statistically consistent with zero (0.0 ± 0.3 at 90% confidence interval), indicating no ion loss.

E. Rate constants

Reaction rate constants for the formation of reaction products are calculated by fitting the loss rate of $C_2D_2{}^+$ ions and dividing it by the concentration of the neutral reactant in the experiment. Table I shows the calculated overall rate constants and statistical uncertainties for $C_2D_2{}^+ + DC_3D_3$ and $C_2D_2{}^+ + H_2C_3H_2$. The results are roughly three times larger than the expected rate constants calculated by the average dipole orientation (ADO) model. We attribute this over-estimate to the inaccuracy of our absolute pressure measurement with our Bayard-Alpert gauge at the 10^{-9} Torr scale.

TABLE I. Calculated reaction rate constants, k, determined by fit of $C_2D_2{}^+$ loss. The reported uncertainties are derived from the 90% confidence interval of the fit (purely statistical) and do not account for possible inaccuracies in the neutral concentration measurement.

Neutral reactant	$k\left(10^{-9}\frac{\mathrm{cm}^3}{\mathrm{s}}\right)$
Propyne (DC_3D_3)	6(1)
Allene ($H_2C_3H_2$)	6(1)

S2. THEORY

A. Propyne + $C_2H_2^+$

1. *Reaction mechanism*

We have constructed a potential energy surface (PES) for the reaction of propyne and acetylene cation using the CCSD(T)/ANO1//CCSD(T)/ANO0 hybrid method mentioned in the main text [2, 3]. It should be noted that the experiments described in the main text were performed with d_4-propyne and d_2-acetylene, while this PES was constructed with d_0-propyne and d_0-acetylene, but no relevant qualitative features of the surface would be changed by isotopic substitution.

The significant presence of $C_5D_5^+$ in the observed products is indicative of the formation of an bound complex between the two reactant species. Because the ionization potential of C_2H_2 is higher than that of propyne, the initial step of the reaction is anticipated to be a charge transfer from the acetylene to the propyne. The two species then associate on the ground state potential energy surface, forming $C_5H_6^+$. Under the very low pressure conditions of the experiment, the loss of energy through collisions is negligible. As a result, the $C_5H_6^+$ intermediates formed have internal energies (90-96 kcal/mol above the many minima on the surface) sufficient to overcome all (intermediate) barriers leading to stable products (see Figure S6).

As seen in Figure S6, **INT0** is produced first on the ground state PES from the association of propyne cation and C_2H_2. **INT0** then quickly isomerizes to **INT1** through a very small barrier of 1.4 kcal/mol (roughly 0.06 eV). There are two possible pathways from **INT1**: it can eliminate an H-atom via **TS1H** leading to **PRD1** or undergo a 1,2 H-shift through

TS12 leading to **INT2**. The latter step overcomes a much lower barrier (about 20 kcal/mol lower than the former), suggesting that it is dominant.

INT2 can further react in three ways: (i) a direct, ring-opening mechanism via **TS24** to yield **INT4**; (ii) an indirect mechanism where a 1,2-H-migration through **TS23** leads to **INT3**, which subsequently undergoes ring-opening through the low-lying **TS34** to yield **INT4**; and (iii) an isomerization via **TS28** to **INT8**, which can then dissociate via a barrierless pathway to **PRD4** (C_2H_2 and allene cation), but energetically prefers to undergo the reverse reaction to **INT2**.

Once produced, **INT4** can isomerize to **INT5** via 1,2-H-migration though **TS45**. Here, the reaction path branches again. A 1,6 ring closure of **INT5** through **TS58** leads to the resonance stabilized cyclopentadiene cation, **INT8**, which can subsequently undergo H-loss via a barrierless pathway to form cyclic $C_5H_5^+$, **PRD5**. The alternative pathway is a 1,3-ring-closure of **INT5** via **TS56**, forming **INT6**.

INT6 can then either cleave a C-C bond via a barrierless pathway to form **PRD2** (cyclopropenyl cation, cyc-$C_3H_3^+$, and vinyl radical, C_2H_3) or form **PRD3** ($C_5H_5^+$ and hydrogen atom) by first undergoing a 2,3-H-migration through **TS67** to form **INT7**, which then loses a hydrogen by **TS7H**.

In summary, the $C_5H_6^+$ intermediates produced on the ground state PES have enough energy to easily pass over all barriers and undergo fast processes that terminate in several products detected in the experimental setup: $C_3H_3^+$,$C_3H_4^+$, and $C_5H_5^+$. It is anticipated that this set of reactions is so rapid that any initial isotopic distribution is nearly completely scrambled by the time products are formed. Chemical kinetics calculations employing this surface can then be performed to determine product yields.

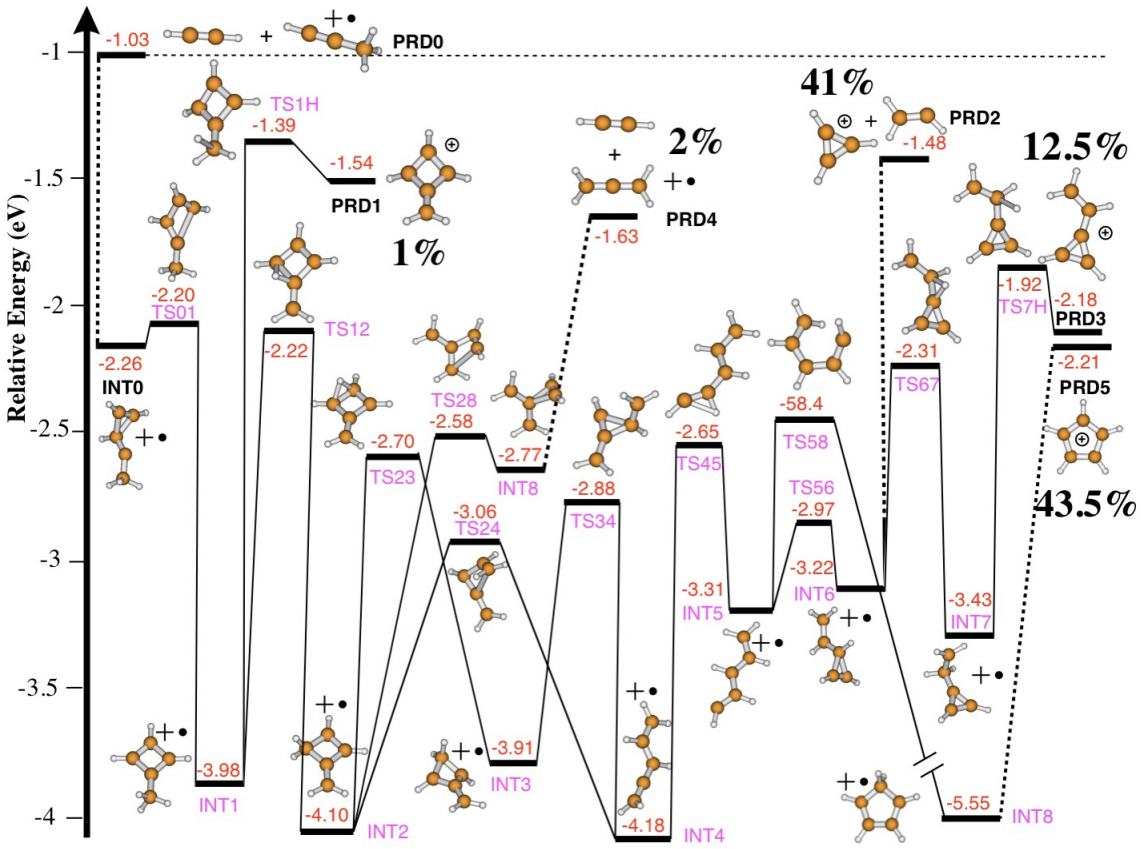

FIG. S6. Potential energy surface for the association of propyne and acetylene cation, computed using the CCSD(T)/ANO1//CCSD(T)/ANO0 hybrid method discussed in the main text. Theoretical product branching ratios obtained by master-equation simulations are indicated in bold.

2. *Statistical chemical kinetics analysis*

Assuming that the experimental conditions are collisionless and non-thermal (the initial energy distribution is represented as a delta function of the post charge-transfer energy), the potential energy surface and rovibrational parameters obtained via quantum chemistry can then be used for chemical kinetics analysis.

A chemical kinetic master-equation under typical conditions which describes the time evolution of the reaction system is given by [4]:

$$\frac{\partial C_i}{\partial t} = \sum_{m=1}^{N} C_m k_{i \leftarrow m}(E, J) - \sum_{i=1}^{N} C_i k_{m \leftarrow i}(E, J). \tag{1}$$

Equation 1 can be cast into matrix form:

$$\frac{\partial}{\partial t}C = \mathbb{M}C, \tag{2}$$

where C is the vector of concentrations of various species, $k_{m\leftarrow i}$ is the microcanonical rate coefficient for isomerization (or dissociation) from species i to species m, and $\mathbb{M}$ is the non-symmetric matrix of rate coefficients, which has dimension N.

$\mathbb{M}$ can be diagonalized to obtain a full set of eigenvalues (Λ) and eigenvectors ($\mathbb{U}$). Concentrations of various species (including intermediates and products) can then be computed as follows:

$$C_i(t) = \mathbb{U}\mathrm{e}^{\Lambda t}\mathbb{U}^{-1}C_i(t=0). \tag{3}$$

In a closed reaction system, there is only one zero eigenvalue (and $N-1$ negative eigenvalues). The eigenvector associated with $\lambda_1 = 0$ contains concentrations (or yields) of all products at the steady-state condition (i.e. at long reaction times).

For a tight, well-defined transition state (TS), RRKM theory [5, 6] is used to compute the microcanonical rate coefficients (Eq. 4); for a loose TS, micro-variational RRKM theory [7, 8] that minimizes sums of quantum states through the dividing surface is employed instead (Eq. 5).

$$k(E,J) = \frac{\sigma}{h}\frac{G^{\ddagger}(E-E_0,J)}{\rho(E,J)}, \tag{4}$$

$$\min(k(E,J)) = \frac{\sigma}{h}\frac{\min(G^{\ddagger}(E-E_0,J))}{\rho(E,J)}, \tag{5}$$

where h is Planck's constant, σ is the reaction path degeneracy, E is the total internal energy, E_0 is the barrier height (including zero-point energy corrections), $G^{\ddagger}$ is the sum of rovibrational quantum states for a TS, and ρ is the density of rovibrational quantum states for a reactant.

Assuming that both reactants and transition states can be approximated as a symmetric tops, the total rovibrational $G^{\ddagger}$ and ρ can be obtained by convolving vibrational and rotational quantum states:

$$G^{\ddagger}(E,J) = \int_0^E G^{\ddagger}_{\mathrm{vib}}(E-E_{\mathrm{rot}})\rho^{\ddagger}_{\mathrm{rot}}(E_{\mathrm{rot}})dE_{\mathrm{rot}}, \tag{6}$$

$$\rho(E,J) = \int_0^E \rho_{\rm vib}(E - E_{\rm rot})\rho_{\rm rot}(E_{\rm rot})dE_{\rm rot}, \tag{7}$$

$$E_{\rm rot} = \bar{B}J(J+1) + (A - \bar{B})K^2 : |K| \leq J. \tag{8}$$

For the motion of the light H atom, quantum mechanical tunneling effects can become important, especially at low temperature. Assuming an asymmetric Eckart potential, $k(E,J)$, the tunneling correction, can be given by [9, 10]:

$$k(E,J) = \frac{\sigma}{h}\frac{\int_0^E P(x)_{\rm Eckart}\rho^{\ddagger}(E-x,J)dx}{\rho(E,J)}, \tag{9}$$

where P(x) is the asymmetric Eckart tunneling probability.

3. Product Yields

The above chemical kinetics analysis provides theoretical product yields of 1% **PRD1** ($H + C_5H_5^+$), 2% **PRD4** (C_2H_2 + allene cation), 12.5% **PRD3** ($H + C_5H_5^+$), 41% **PRD2** (CH_2CH + c-$C_3H_3^+$), and 43.5% **PRD5** ($H + C_5H_5^+$). As it is impossible to distinguish between cation isomers in this experimental setup, we can only compare the gross empirical formulas: 2% $C_3H_4^+$, 41% c-$C_3H_3^+$, and 57% $C_5H_5^+$, or a product ratio of roughly 2:3 c-$C_3H_3^+$ to $C_5H_5^+$. These product yields do not quantitatively agree with the experimental product ratios of roughly 8:3 $C_3D_3^+$ to $C_5D_5^+$. More problematic are the experimentally observed $C_3D_4^+$ intermediates that are later consumed by secondary reactions - a feature not predicted by the theoretical simulation. There are a couple plausible explanations of these discrepancies. First, it is possible that the dynamics of this reaction, perhaps due to the experimental environment or some inherent feature of the reactive surface, behaves non-statistically, leading to the discrepancy between the long-lifetime yields. Second, we have not considered the possibility of a long-range charge transfer between acetylene cation and propyne that does not lead to the formation of the bound complex, and instead results in separated acetylene and propyne cation. There is clearly a pathway in the experimental results that yields a significant quantity of $C_3D_4^+$ intermediates that are later consumed by secondary reactions. While it is possible that this is a result of **PRD2** on the PES shown in Figure S6, given that the experimental yield of $C_3D_4^+$ is at one point greater than that

of $C_5D_5^+$ (which is not found in the theoretical results), it is more reasonable to conclude that the charge transfer range is slightly larger than the collisional capture range, and the yield of $C_3D_4^+$ is thus under-predicted by our theoretical model. Unfortunately, we know of no reliable way to predict the ratio of charge transfer reactions that lead to the bounded complex vs. those that lead to charge exchange.

B. Allene + $C_2D_2^+$

1. Reaction mechanism

Figure S7 displays the potential energy surface for the proposed mechanism of the reaction between d_0-allene and d_2-acetylene cation using the mHEAT+ model chemistry [11]. The acetylene cation and neutral have been treated with only harmonic ZPE corrections, due to difficulties arising from Renner-Teller effects on the cation. The relatively small ionization potential of allene permits long range charge transfer between the d_0-allene and the d_2-acetylene cation, forming allene cation and acetylene neutral (**INT1**). Assuming the internal energy released during the charge transfer is available to the allene cation, it then rapidly isomerizes to vinylmethylene cation (**INT2**) via a 1,2-H-shift through **TS1**. Vinylmethylene cation then faces only a small barrier to cyclize to the cyclopropene cation (**INT3**) via a 1,3-ring-closure (**TS2**). Then, if indeed all the internal energy is localized on the allene cation, cyclopropene cation can lose a hydrogen by tunneling through **TS3** to form a post-reaction complex where the lone hydrogen is weakly bound to the resonance stabilized cyclopropenyl cation (**PRC1**). Upon losing this hydrogen, the reaction products, cyclopropenyl cation and hydrogen atom, are formed (**PRD1**). These products are exothermic to the initial reactants by 0.016 eV (1.56 kJ/mol). The 95% confidence interval for the mHEAT+ model chemistry is roughly 0.015 eV (1.5 kJ/mol), meaning that the exothermicity of the products remains qualitatively the same even within a 2σ error (thermal internal energy of the allene reactants non-withstanding). In the case of non-deuterated acetylene (for which enthalpies of formation exist in the Active Thermochemical Tables [12]), the ATcT reaction enthalpy at 0 K is -0.7 ± 1.3 kJ/mol.

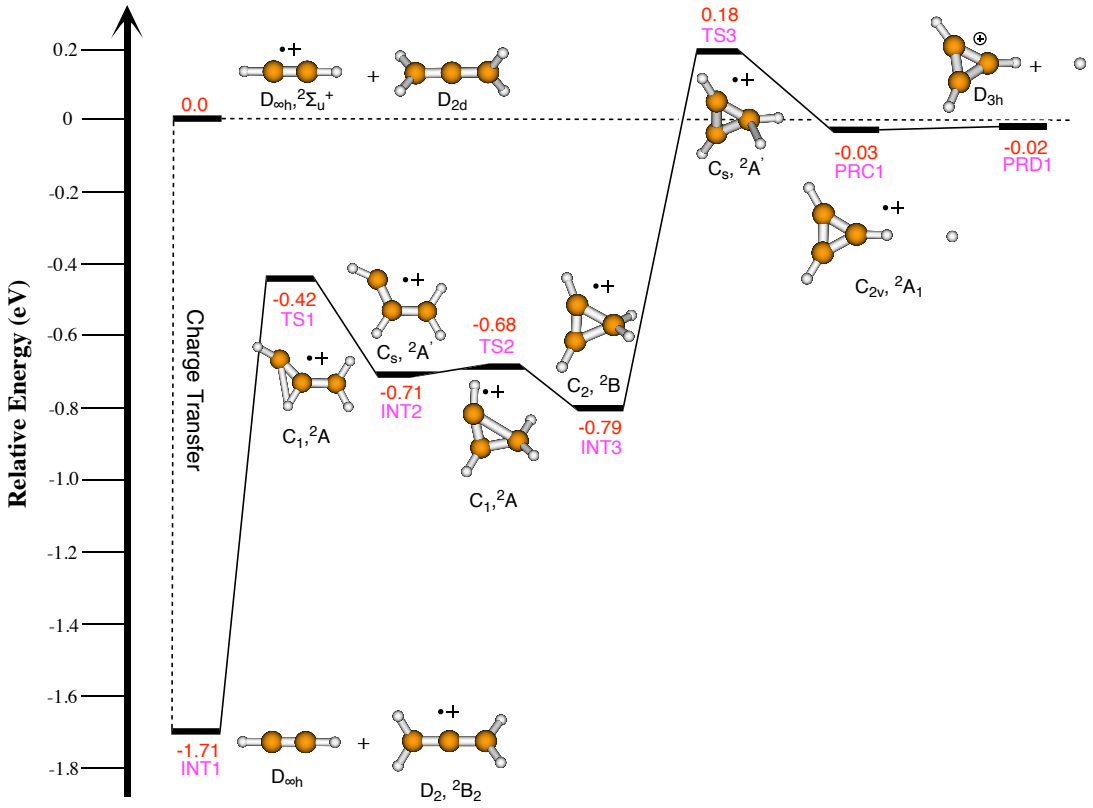

FIG. S7. Potential energy surface of the reaction between d_2-acetylene cation and d_0-allene neutral, calculated using the mHEAT+ model chemistry.

2. *RRKM tunneling rate*

To test if the proposed mechanism for the reaction between allene and acetylene cation is a feasible explanation for the observed products, we have performed a rudimentary RRKM simulation of the tunneling rate that leads to the post-reactive complex. In this model, the reactant is taken to be **INT1**, the allene cation, the transition state is **TS3**, and the products are **PRD1**. We employed semiclassical TST to obtain the density of states for the TS, which accounts for VPT2 anharmonicity, coupling between the reaction coordinate and vibrational degrees of freedom, and quantum tunneling. Assuming 100% of the charge transfer energy is localized on the allene cation, the microcanonical rate coefficient of tunneling from **INT3**

to **PRD1** is 21.7 s^{-1}. A more detailed model of this mechanism and the rates associated is saved for later work, but the rather basic treatment above is sufficient to show that while this reaction is certainly not fast (in the context of ion-molecule reactions), it is fast enough that the kinetics are dominated by the bimolecular rate associated with the "collision" of acetylene cation and allene neutral in the first place, and that tunneling occurs well within the timescale of the experiment.

C. Theoretical program packages

All quantum chemical calculations were performed with the CFOUR package [13]. The kinetics calculations were performed using the MultiWell program suite [14].

---

[1] P. C. Schmid, J. Greenberg, M. I. Miller, K. Loeffler, and H. J. Lewandowski. An ion trap time-of-flight mass spectrometer with high mass resolution for cold trapped ion experiments. *Rev. Sci. Instrum.*, 88(12):123107, 2017.

[2] Krishnan Raghavachari, Gary W. Trucks, John A. Pople, and Martin Head-Gordon. A fifth-order perturbation comparison of electron correlation theories. *Chemical Physics Letters*, 157(6):479 – 483, 1989.

[3] Rodney J. Bartlett, J.D. Watts, S.A. Kucharski, and J. Noga. Non-iterative fifth-order triple and quadruple excitation energy corrections in correlated methods. *Chemical Physics Letters*, 165(6):513 – 522, 1990.

[4] Thanh Lam Nguyen and John F. Stanton. Pragmatic solution for a fully e,j-resolved master equation. *The Journal of Physical Chemistry A*, 124(15):2907–2918, 2020. PMID: 32207958.

[5] R. A. Marcus. Unimolecular dissociations and free radical recombination reactions. *The Journal of Chemical Physics*, 20(3):359–364, 1952.

[6] R. A. Marcus. Dissociation and isomerization of vibrationally excited species. iii. *The Journal of Chemical Physics*, 43(8):2658–2661, 1965.

[7] Donald G. Truhlar and Bruce C. Garrett. Variational transition-state theory. *Accounts of Chemical Research*, 13(12):440–448, 1980.

[8] William L. Hase. Variational unimolecular rate theory. *Accounts of Chemical Research*, 16(7):258–264, 1983.

[9] William H. Miller. Tunneling corrections to unimolecular rate constants, with application to formaldehyde. *Journal of the American Chemical Society*, 101(23):6810–6814, 1979.

[10] Thanh Lam Nguyen, John F. Stanton, and John R. Barker. A practical implementation of semi-classical transition state theory for polyatomics. *Chemical Physics Letters*, 499(1):9 – 15, 2010.

[11] James H. Thorpe, Chris A. Lopez, Thanh Lam Nguyen, Joshua H. Baraban, David H. Bross, Branko Ruscic, and John F. Stanton. High-accuracy extrapolated ab initio thermochemistry. IV. A modified recipe for computational efficiency. *J. Chem. Phys.*, 150(22):224102, 2019.

[12] Ruscic, B. and Bross, D. H., Active Thermochemical Tables (ATcT) values based on ver. 1.122g of the Thermochemical Network (2019); available at ATcT.anl.gov.

[13] CFOUR, a quantum chemical program package written by J.F. Stanton, J. Gauss, L. Cheng, M.E. Harding, D.A. Matthews, P.G. Szalay with contributions from A.A. Auer, R.J. Bartlett, U. Benedikt, C. Berger, D.E. Bernholdt, Y.J. Bomble, O. Christiansen, F. Engel, R. Faber, M. Heckert, O. Heun, M. Hilgenberg, C. Huber, T.-C. Jagau, D. Jonsson, J. Juslius, T. Kirsch, K. Klein, W.J. Lauderdale, F. Lipparini, T. Metzroth, L.A. Mck, D.P. O'Neill, D.R. Price, E. Prochnow, C. Puzzarini, K. Ruud, F. Schiffmann, W. Schwalbach, C. Simmons, S. Stopkowicz, A. Tajti, J. Vzquez, F. Wang, J.D. Watts and the integral packages MOLECULE (J. Almlf and P.R. Taylor), PROPS (P.R. Taylor), ABACUS (T. Helgaker, H.J. Aa. Jensen, P. Jrgensen, and J. Olsen), and ECP routines by A. V. Mitin and C. van Wllen. For the current version, see http://www.cfour.de.

[14] J. R. Barker, T. L. Nguyen, J. F. Stanton, C. Aieta, M. Ceotto, F. Gabas, T. J. D. Kumar, C. G. L. Li, L. L. Lohr, A. Maranzana, N. F. Ortiz, J. M. Preses, J. M. Simmie, J. A. Sonk, and P. J. Stimac; MultiWell-Software Suite; J. R. Barker, University of Michigan, Ann Arbor, Michigan, USA, 2018, http://clasp-research.engin.umich.edu/multiwell/.